Speculations on the impact of subduction initiation on the Earth System

F.O. Marques[1,2*], B.J.P. Kaus[2]

[1] *Universidade de Lisboa, 1749-016 Lisboa, Portugal*

[2] *Institut für Geowissenschaften, Johannes Gutenberg-Universität, Mainz, Germany*

*Corresponding author. Tel.: 351 217500000; Fax: 351 217500064

E-mail address: fomarques@fc.ul.pt

Abstract

The physics of subduction initiation can be studied with numerical models of lithosphere dynamics, to the extent where we can now test the potential consequences of a catastrophic subduction initiation event on the Earth system. The South American Atlantic passive margin is here used to show that, once subduction has catastrophically initiated there, a major geodynamic reconfiguration of the South American plate (SAm) is likely to take place: (1) compression in the east will be inverted to extension, because ridge push will be replaced by subduction rollback and trench retreat; (2) compression in the west will be inverted to extension due to absolute rollback; and (3) without buttressing from the east and west, the Andes will collapse. Extension at both margins of continental SAm will produce two new volcanic arcs, several thousands of kilometres long each, bounded by trenches and two new back-arc basins. The spreading rate of the Mid-Atlantic Rift will significantly increase, because of the cumulative effect of ridge-push and slab-pull in the same direction. The substantially increased volcanism all around SAm and in the MAR will most likely release massive amounts of greenhouse and toxic gases into the atmosphere and oceans, which might lead to major oceanic and atmospheric circulation changes.

We present new numerical modelling that supports the proposed evolution of the SAm after subduction has catastrophically initiated at its eastern passive margin.

Keywords: subduction initiation; passive margin; geodynamic setting; global changes; biotic crisis; Earth system; numerical modelling

1. Introduction

When discussing global changes and impact on life on Earth, one has to account for the time range of the process: it must be large scale and catastrophic (short time), so that the biosphere does not have the time to adapt to the new conditions, especially in atmosphere and hydrosphere. We can look at this relationship as a Deborah number (*De*): the time of subduction initiation divided by the characteristic time living beings take to adapt to new conditions. If $De < 1$, then catastrophic subduction initiation at a passive margin (< 1 Ma) is a process capable of producing a biotic crisis. Otherwise, there is time for adaptation because environmental changes take place slowly over a long period of time (>> 1 Ma). Therefore, here we concentrate on the fast end-member of subduction initiation, the catastrophic initiation capable of producing sudden global changes and impact on life on Earth. Using well-known constitutive equations and parameters determined experimentally (e.g. Weertman, 1968; Hirth and Kohlstedt, 2003; Korenaga and Karato, 2008), here we show numerically that subduction can initiate in less than 1 Ma, which seems insufficient time for a great part of the biosphere to adapt to extreme new conditions (Wignall and Twitchett, 1996; Wignall, 2001). We conclude that catastrophic subduction initiation at a passive margin can be responsible for mass extinctions.

At the surface, subduction is responsible for catastrophic events like explosive volcanism, large earthquakes and major tsunamis, which obviously impact human societies. Although omnipresent, mature subduction does not seem capable of triggering fast global changes that

would impact the whole Earth system. In contrast, subduction initiation at a passive margin can be catastrophic, in terms of time and transformations.

McKenzie (1977) mathematically analysed the problem of subduction initiation at a passive margin, and concluded that the development of a new trench and sinking slab occurs through a finite amplitude instability, because elastic and frictional forces prevent trenches from arising spontaneously. This means that an external force is needed to initiate subduction. The compressive stress required is about 80 MPa, and the rate of approach must be greater than about l.3 cm/yr. Two immediate sources of compressive stress in a passive margin are ridge-push and topography push from the passive margin. The difference in mean density between continental and oceanic crusts produces a horizontal force (e.g. Niu et al., 2003; Marques et al., 2014) similar to the push caused by elevated mid-oceanic ridges (ridge-push). If the difference in elevation between a continent and adjacent ocean is 7 km, with 2 km above sea level and 5 km below (as at the Brazilian margin), it can maintain a compressive stress of 85 MPa. If to these stresses we add the stresses due to Andean topography and deep roots, which can amount to 100 MPa if the estimated 1E13 N/m (e.g. Artyushkov, 1987; Husson et al., 2008) are integrated along a 100 km thick lithosphere, then the South American Plate (SAm) seems the best place for subduction to initiate at a passive margin. The probability of subduction to initiate along the eastern American Atlantic margins has been numerically evaluated by Nikolaeva et al. (2011) and Marques et al. (2013), who concluded that the SE Brazilian margin has the highest probability for subduction initiation to occur there. According to Marques et al. (2013), subduction could likely be initiating at the Brazilian passive margin, because of additional forcing by the current massive Andean Plateau and its very deep crustal roots (which are hot and of low-density). Given the favourable geodynamic setting for subduction initiation, here we concentrate on SAm's possible future evolution.

If the current theoretical analyses and the physics governing subduction initiation are

accepted, then a major question arises: what is the impact of subduction initiation on the Earth system? The answer to this question is the aim of this article. We use current knowledge about the SAm and numerical models to predict what will happen to the SAm in the future, and evaluate the impact these changes can have on the Earth system if subduction initiates catastrophically at a passive margin.

The main premises of this work relate to (1) catastrophic subduction initiation at a passive margin, (2) the rheology of the sub-lithospheric mantle, (3) the support of mountain belts (buttressing), and (4) the motion of the subduction hinge:

(1) Catastrophic subduction initiation – Hall et al. (2003) and Nikolaeva et al. (2010) have analysed numerically subduction initiation at a passive margin, and both have concluded that self-sustained subduction can take off in about 1 Ma (see also Lu et al., 2015). Nikolaeva et al. (2010) carried out a parametric study that shows that the thickness of the continental lithosphere can lead to catastrophic (< 1 Ma) subduction initiation at a passive margin (cf. their Fig. 6). Using the current geological and geophysical knowledge of the SAm, we further tested the effects of rheology (diffusion and dislocation creeps) and activation volume on the velocity of subduction initiation.

(2) Rheology of the sub-lithospheric mantle – the rheological properties of the mantle are critical to its dynamics; however, fundamental issues as the dominant flow mechanisms are still not consensual. Laboratory studies and geophysical and geological data indicate that both diffusion and dislocation creep can occur in the mantle (Karato and Wu, 1993). However, according to Bürgmann and Dresen (2008), broadly distributed deformation in the asthenosphere probably occurs by dislocation creep, with a stress-dependent power-law rheology. Therefore, we used dislocation creep (power-law creep) as the rheology of the sub-lithospheric mantle in our models. However, we tested the influence of rheological law (diffusion or dislocation creep), and of activation volume on subduction initiation (see also Billen and Hirth, 2005, 2007).

(2) Buttressing – it is long known that mountains like the Himalaya or the Andes are supported by the surrounding lithosphere; if this support vanishes, the mountain belt collapses. This is what has happened to all orogens worldwide and through the Earth's history; when convergence and compressive forces cease, the mountain belt collapses and the deep continental roots isostatically rebound, denudation removes the topographic relief, and the Moho returns to its normal position at 30-40 km depth.

(3) Motion of the trench – It is now well established that the large majority of N-S trenches and their associated subduction zones are found at, or very near, the margins of the Pacific Ocean. Exceptions are the much smaller Indonesian, Caribbean, and Scotia trenches. Along the N-S portions of the Pacific trenches, all slabs go down so as to slope away from the Pacific margins. Given that the Atlantic and the Indian oceans have been opening in an approximately E-W direction since the Mesozoic, it follows that the Pacific plate must have shrunk by a corresponding length during the same period of time, which means that the trenches have retreated (e.g. Elsasser, 1971; McKenzie, 1977). Fig. 1 illustrates how this can happen: after subduction is initiated and is self-sustained, the sinking of the oceanic slab is dominated by its negative buoyancy. Under the pull of gravity, the slab tends to rotate vertically and oceanwards, which is the concept of slab rollback. Slab rollback induces trench retreat oceanwards, and, in order to fill the gap, the overriding plate either drifts or stretches and opens a back-arc basin. The force resulting from trench retreat was called trench suction by Forsyth and Uyeda (1975). Trench retreat has even been suggested to be responsible for the break-up of supercontinents (e.g. Bercovici and Long, 2014), and might currently be responsible for the shrinking of the Pacific. However, the scheme in Fig. 1 is valid only if the oceanic plate has no horizontal displacement (fixed at the right end in Fig.1). This might not be the case if the oceanic plate could move, e.g. by having a mid-ocean rift. Therefore, we analysed this possibility by running simulations with and without a mid-ocean rift.

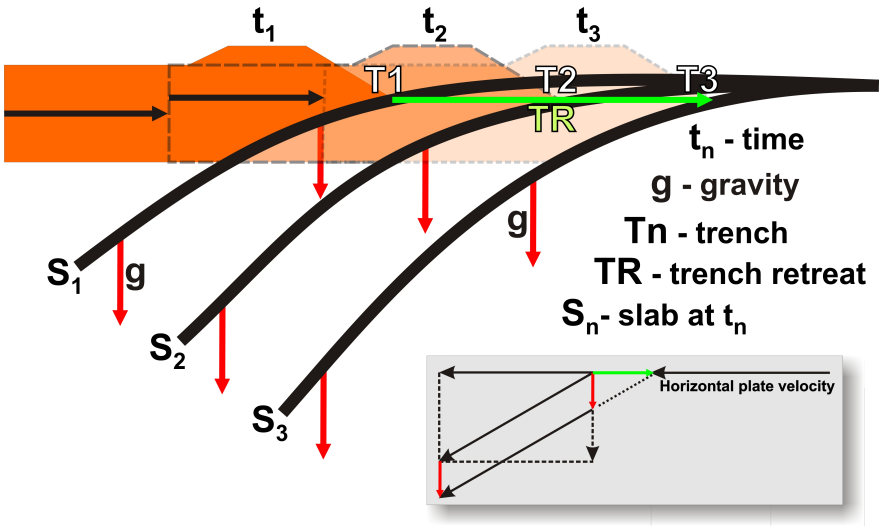

Figure 1. Sketch illustrating slab rollback and consequent trench retreat. The overriding continent may either drift or rift, in the latter case to form a back-arc basin.

Natural examples (e.g. Gvirtzman and Nur, 1999; Rosenbaum and Lister, 2004; Schellart et al., 2006; Spakman and Hall, 2010) and theoretical analysis of subduction initiation at a passive margin (e.g. Faccenna et al., 1999; Nikolaeva et al., 2010, 2011; Marques et al., 2013, 2014) have shown that rollback is a natural consequence immediately following subduction initiation (e.g. Kincaid and Olson, 1987; Hall et al., 2003; Kincaid and Griffiths, 2003; Funiciello et al., 2003a, b, 2006, 2008; Gurnis et al., 2004; Schellart, 2005, 2008, 2010, 2011; Stegman et al., 2006; Schellart et al., 2006, 2007, 2008, 2011; Lallemand et al., 2008; Di Giuseppe et al., 2008, 2009; Capitanio et al., 2010; Schellart and Rawlinson, 2010; Stegman et al., 2010a, b; Rodríguez-González et al., 2012, 2014; Niu, 2014; Holt et al., 2015). Therefore, the passive margin, originally (before subduction initiation) under compression due to ridge-push and margin topography, may undergo extension when self-sustained subduction initiates (Fig. 1). In order to test this hypothesis, we used numerical modelling as presented below.

2. Geodynamic setting

The SAm (Fig. 2) is bounded in the north and south by two transform faults, in the east

144 by the MAR axis, in the west by the Chile trench, and at the base by the asthenosphere.

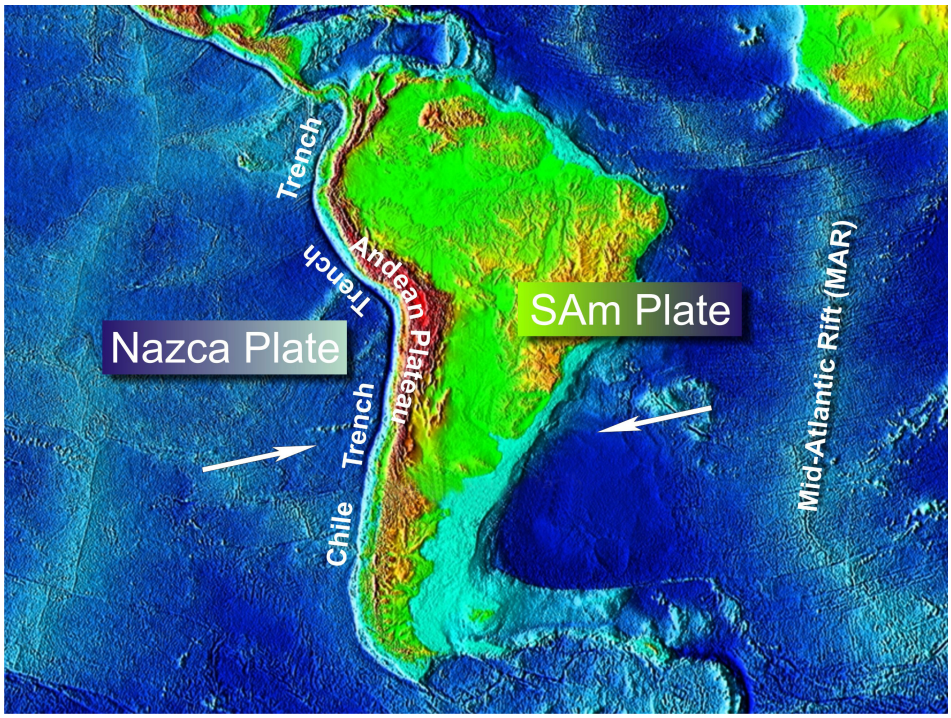

145

146 *Figure 2. Simplified present-day tectonic setting of the South America lithospheric plate. Arrows*
147 *represent horizontal plate motion with the African plate fixed. Background image is a*
148 *shaded relief image from ETOPO5 digital data*
149 *(http://www.ngdc.noaa.gov/mgg/global/relief/etopo5/images/tif/slides_t/slide15.tif).*

150

151 The SAm has two major topographic reliefs along its eastern (MAR) and western
152 (Andes) boundaries (Fig. 2), which produce topographic forces that keep the SAm under
153 compression (e.g. Coblentz and Richardson, 1996). The SAm's western boundary is currently
154 being pushed from the west by relative subduction roll-forth (e.g. Russo and Silver, 1996), which
155 works as an effective backstop. Otherwise the Andes would collapse to the west. Push from the
156 west coupled with MAR push from the east guarantees the existence of the Andes, in particular
157 the impressive Andean Plateau, by supporting the mountain belt from east and west.

158 The Andes are hot and weak, therefore: (1) they can spread horizontally, and therefore
159 push the SAm plate eastwards; and (2) they cannot directly transmit the stresses born from

relative roll-forth of the Chile Trench into the rigid SAm, because they deform internally thus dissipating the stresses born from a relatively advancing trench. The continental SAm is thick and rigid, and therefore a privileged guide to the stresses imposed from the east (MAR) and west (Andes). Because the Brazilian shield and the Atlantic oceanic lithosphere are very strong, they convey stress into the weak (thinned and rifted) Brazilian margin, where continental and oceanic lithospheres meet and strain should preferentially concentrate. Here, the stresses can be increased by the Brazilian Plateau (almost 3,000 m of altitude close to the Brazilian margin), as a result of the density contrast and the more than 7,000 m elevation difference between continent (less dense) and ocean (denser) (Marques et al., 2014). The sum of the forces acting on SAm has been numerically shown to be enough to initiate subduction at a passive margin (Nikolaeva et al., 2011; Marques et al., 2013), and should therefore be enough to break the Brazilian margin and initiate self-sustained subduction. Once this happens, a series of events will take place that affects plate kinematics and force balance, and thus the SAm's geodynamic configuration (Figs. 2, 3). Currently the SAm is compressed from west and east by Andes and MAR opposing pushes (e.g. Assumpção, 1992; Coblentz and Richardson, 1996; Cogné et al., 2011, 2012, 2013)(Fig. 2a), but this stress state can dramatically change with subduction initiation.

Considering the general case of a 2-D Earth and steady state, the force balance on a plate can be written as:

$$F_{rp} + F_{sp} + F_{md} + F_{ff} + F_{bf} + F_{ip} = 0$$

where F_{rp} = ridge push; F_{sp} = slab pull; F_{md} = mantle drag; F_{ff} = fault friction; F_{bf} = boundary forces exerted by other plates; F_{ip} = intra-plate forces.

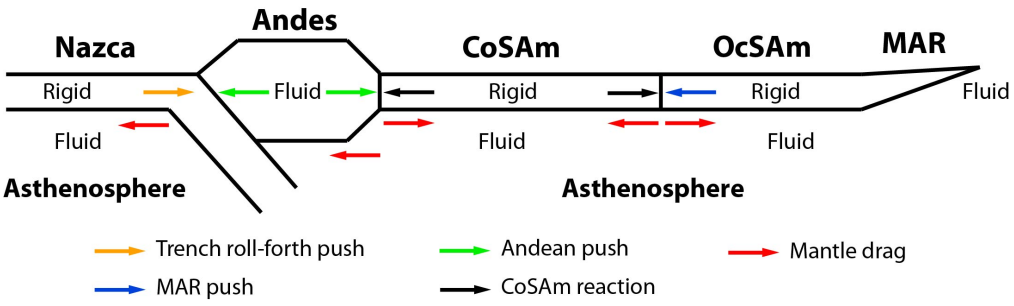

Figure 3. Sketch, in vertical cross-section, of the 2-D force balance in the South American Plate at steady state.

In the particular case of the SAm (Fig. 3), the forces can be evaluated as follows: (1) once we know the average age of the oceanic crust along the SAm's continental margin, we can estimate F_{rp}. (2) $F_{sp} = 0$ because the contribution of the slab-pull force to the dynamics of the SAm has been considered negligible (e.g. Meijer and Wortel, 1992; Coblentz and Richardson, 1996). The topographic forces like MAR-push, Brazilian Plateau-push, and Andes-push are the main contributors to the intraplate stress field. (3) F_{md} is a force that cannot be neglected, but, as a first approximation, we will assume it to be a constant resistive force. (4) F_{ff} occurs at the northern and southern SAm's boundaries, but it is most probably negligible, because transform faults are typically weak (e.g. Zoback, 1991), and their area is much smaller than the area subjected to F_{md}. (5) F_{bf} corresponds to the Andean push, which can be estimated. (6) F_{ip} is mostly restricted to the Brazilian Plateau, but given its small size compared to the entire SAm, the topographic force is relevant locally. We conclude that only three forces are relevant regarding the SAm: the MAR push (FMAR-p), the Andean push (FAndes-p) and the mantle drag (FMd).

3. Numerical Modelling

The objective of our numerical modelling was not to investigate subduction initiation at a passive margin per se, but rather to test back-arc rifting in the overriding continental plate, by

206 slab rollback and trench retreat immediately following subduction initiation. Therefore, the
207 model was designed so as to guarantee that subduction initiates at the model Brazilian margin, in
208 a model setup similar to the SAm in a cross-section from the Altiplano to the MAR through the
209 SE Brazilian margin. Here the continent and the ocean are about 3,000 km long each.
210
211 *3.1. Numerical code and boundary conditions*
212 The numerical code employed here, MVEP2, is a further-development of
213 MILAMIN_VEP, which has been described in detail elsewhere (Kaus, 2010; Thielmann and
214 Kaus, 2012; Schmeling et al., 2008). For completeness, a brief summary is provided in Johnson
215 et al. (2014).
216 The incompressible Stokes system of equations is solved with the extended Boussinesq
217 approximation. Both shear heating and adiabatic (de)compression are taken into account in the
218 energy equation. Density in the models is a function of rock type, pressure and temperature. A
219 viscoplastic constitutive relationship is used, in which the dominant rheology is diffusion creep,
220 dislocation creep or plastic yielding. For mantle rocks we used dislocation creep (Hirth and
221 Kohlstedt, 2003), whereas the crust was assumed to have a wet quartz rheology (Ranalli, 1995).
222 The constitutive equations used in the present modelling have the form:
223
224 $\dot{\varepsilon} = \sigma^n * fH_2O^r * A * \exp\left[(-E + PV)/R * T\right]$ for dislocation creep
225 and
226 $\dot{\varepsilon} = \sigma^n * d^{-p} * A * \exp\left[(-E + PV)/R * T\right]$ for diffusion creep
227
228 where A is a constant, n is the stress exponent, d is the grain size, p is the grain size exponent,
229 fH$_2$0 is the water fugacity, r is the water fugacity exponent, E is the activation energy, V is the
230 activation volume, R is the gas constant, and T is the temperature.

231 The parameters in the Arrhenius term reflect the viscosity of the rock, and some have
232 reasonably well constrained values but others do not. This is the case of V for olivine (the major
233 constituent of the mantle), for which experimentally determined values vary significantly,
234 statistically in the range 13±8 cm^3 mol^{-1} (Korenaga and Karato, 2008). In order to be on the
235 conservative side, we used the average value 13 in the present models. However, we tested the
236 effects of varying V on subduction initiation, and present the corresponding graphs below.
237 We also used dry and wet rheologies to simulate water-poor (lithospheric and sub-
238 lithospheric mantles) and water-rich (oceanic and continental crust) rocks, respectively. Note that
239 wet rheology means weaker rock.
240 Cohesion and angle of internal friction control the plastic behaviour. The smaller their
241 values the weaker the rock.
242 With the constitutive equations and parameters from Hirth and Kohlstedt (2003) that we
243 used in the simulations, the viscosity becomes very large in the mantle lithosphere (larger than
244 10^{25} Pa s), whereas strain rates in some other areas are sufficiently high to result in viscosities
245 lower than 10^{16} Pa s. Given that nine orders of magnitude cannot be handled by the numerical
246 code, we imposed viscosity lower and upper cut-offs of 10^{18} and 10^{23} Pa s, respectively (in
247 agreement with what is done in other lithosphere dynamics codes).
248 An overview of the model parameters used in the current set of simulations is given in
249 Table 1.
250
251 Table 1. Summary of model parameters.

Phase	ρ (kg/m^3)	C (MPa)	ϕ (°)	V (cm^3/mol)	Max yield (MPa)	Creep law
OC	3100	5	2	1	50	Wet olivine
SOLM	3300	20	30	15	50	Dry olivine
CC	2850	5	2	0	50	Wet quartzite
SCLM	3250	20	30	15	50	Dry olivine
WLPB	3300	5	2	1	50	Wet olivine
SLM	3300	20	30	13*	50	Dry olivine
VLW	3250	1	1	1	50	Wet quartzite

OC = oceanic crust; SOLM = sub-oceanic lithospheric mantle; CC = continental crust; SCLM = sub-continental lithospheric mantle; WLPB = weak layer at plate boundary; SLM = sub-lithospheric mantle; VLW = vertical lithospheric weakness

** Varied from 6 to 20 in the experiments to test the effects of V*

ρ = density; C = cohesion ; ϕ = angle of internal friction; V = activation volume; Max yield = maximum yield stress regarding plasticity; Creep law = wet and dry olivine from Hirth and Kohlstedt (2003), and wet quartzite from Ranalli (1995)

252

253

254 The governing equations were solved with the 2-D finite element code MVEP2. The code
255 is written in MATLAB, and has been made more efficient by employing the techniques
256 described in Dabrowski et al. (2008). Tracers are used to track material properties, and the code
257 is used in ALE mode with regular remeshing to ensure that elements do not become too
258 distorted. It has been benchmarked for a large number of test problems, as well as against
259 various analytical solutions (e.g. SolCx or weak/strong inclusion setups), as described in a
260 number of publications (Gerya and Yuen, 2007; May and Moresi, 2008; Schmeling et al., 2008;
261 Crameri and Kaus, 2010; Yamato et al., 2011; Crameri et al., 2012; Thielmann and Kaus, 2012).
262 The model employs a computational mesh of 257x257 nodes, which is refined towards
263 the lithosphere, such that there is a resolution of 3.9 km (horizontal) by 2.1 km (vertical) in the
264 lithosphere, and 3.9 by 3.2 km below a depth of 330 km. Compositions are tracked on tracers of
265 which there are initially ~0.8 million. The code injects particles in finite elements that have less

than two particles during a simulation.

The boundary conditions in all models were “free slip” at the bottom and sidewalls, and “free surface ” or “stress free” at the top. Given that topography is due to isostatic equilibrium, and that the boundary condition at the top of the model is “no stress”, topography could build up in the initial stages reproducing to a first order the observed topography in the SAm: higher and positive where the continental crust and lithospheric mantle are thick, still positive but lower where the continental crust and lithospheric mantle are thinner, and negative and deep in the oceanic domain. Later the topography reflected the evolution of the simulations.

In all models, no velocities were imposed at the sidewalls, which means that all simulations were fully driven by gravity.

3.2. Model setup

The 2-D model domain was 6,000 km wide and 1,400 km deep (Figs. 4 and 5). It comprised two domains, one continental and one oceanic , each 3,000 km wide. The contact between oceanic and continental domains had a dip of 45º toward the west, and comprised a 15 km thick weak layer between the continental and oceanic phases. The continental SAm had a lithospheric structure similar to the one deduced from geophysics for the SAm (Heit et al., 2007 for the Andean sector; Artemieva and Mooney, 2001, and Feng et al., 2007 for the remaining lithosphere to the east of the Andes): (1) a deep crust 60 km thick and 600 km wide (model Andean Plateau) bounded by the western wall. East of the model Andean Plateau, the crust was 40 km thick. (2) A sub-continental lithospheric mantle 140 km thick and 700 km wide below the model Andean Plateau, followed to the east by a 150 km thick and 1,600 km wide lithosphere, which finally wedged out to 100 km thick in the last 700 km before the contact with the oceanic plate. The oceanic domain comprised an 85 km thick and 3,000 km wide sub-oceanic lithospheric mantle, capped by a 15 km thick and 3,000 km wide oceanic crust. We are aware

that 15 km might seem too thick, but this is equivalent to the thickness of oceanic crust plus capping sediments near the margin. Additionally, 15 km are needed for the code to properly resolve the phase. Continental and oceanic domains were underlain by a sub-lithospheric mantle till –1,400 km.

In order to complete the model setup, we added two relatively small weak layers: (1) one was oblique, 100 km long and 15 km thick (true orthogonal thickness), along the westward 45º dipping contact between ocean and model SAm; (2) the other was vertical, 20 km thick and 110 km deep, just within the sub-continental lithospheric mantle, therefore with top at –40 km. The inclusion of this vertical lithospheric weakness is justified, because the Brazilian continental lithosphere is deeply cut by lithospheric-scale shear zones (e.g. Vauchez and Tommasi, 2003), many of them approximately parallel to the Brazilian continental margin. They extend from N Uruguay to S Brazil (e.g. Tommasi et al., 1994; Passarelli et al., 2010), some stretch across Central Brazil (e.g. Passarelli et al., 2010), and other deep shear zones occur in NE Brazil (e.g. Vauchez et al., 1995; Vauchez and Tommasi, 2003). Some of these have been reactivated to produce the Cretaceous Basins in NE Brazil (e.g. Matos, 1992), and most of them have subsequently have been reactivated again to produce inversion of the earlier formed basins (e.g. Gurgel et al., 2013; Marques et al., 2014; Nogueira et al., 2015). Current reactivation of the major shear zones has been reported for NE Brazil (e.g. Bezerra and Vita-Finzi, 2000).

We used the following temperature profile in the continental SAm and sub-lithospheric oceanic SAm: linear with a slope of 13 ºC/km from 0 to –100 km; linear with a slope of 0.67 ºC/km from –100 to –400 km, so that temperature was 1500 ºC at 400 km (top of transition zone, experimentally controlled by olivine to spinel phase change); linear with a slope of 0.74 ºC/km from –400 to –670 km, so that temperature was 1700 ºC at 670 km (bottom of transition zone, experimentally controlled by spinel to perovskite + oxides phase change); and linear adiabatic temperature gradient of 0.3 (Ranalli, 1995), so that the temperature increased till the bottom of

316 the model domain (–1,400 km), where initially it was 1919 ºC. In the model including a mid-
317 ocean ridge, the thermal profile in the oceanic domain was that of an oceanic lithosphere from
318 the rift to the continental margin (Turcotte and Schubert, 2014). Thermal boundary conditions
319 were isothermal at the top and bottom (in accordance with the initial geotherm), and flux-free at
320 the side boundaries.

321

322 *3.3. Model results*

323 Here we present the results of three main models: Model 1 – composed of one continent
324 and one ocean without a mid-oceanic rift (MOR), in order to serve as reference for comparison
325 with the model with a MOR. Model 2 – composed of one continent and one ocean with a MOR,
326 to simulate subduction initiation in a section from the Andes to the MAR. Model 3 – similar to
327 Model 2, but with a full Atlantic and part of Africa. The lengths of model SAm and Atlantic are
328 similar to the natural lengths in a section through the Altiplano and SE Brazil.

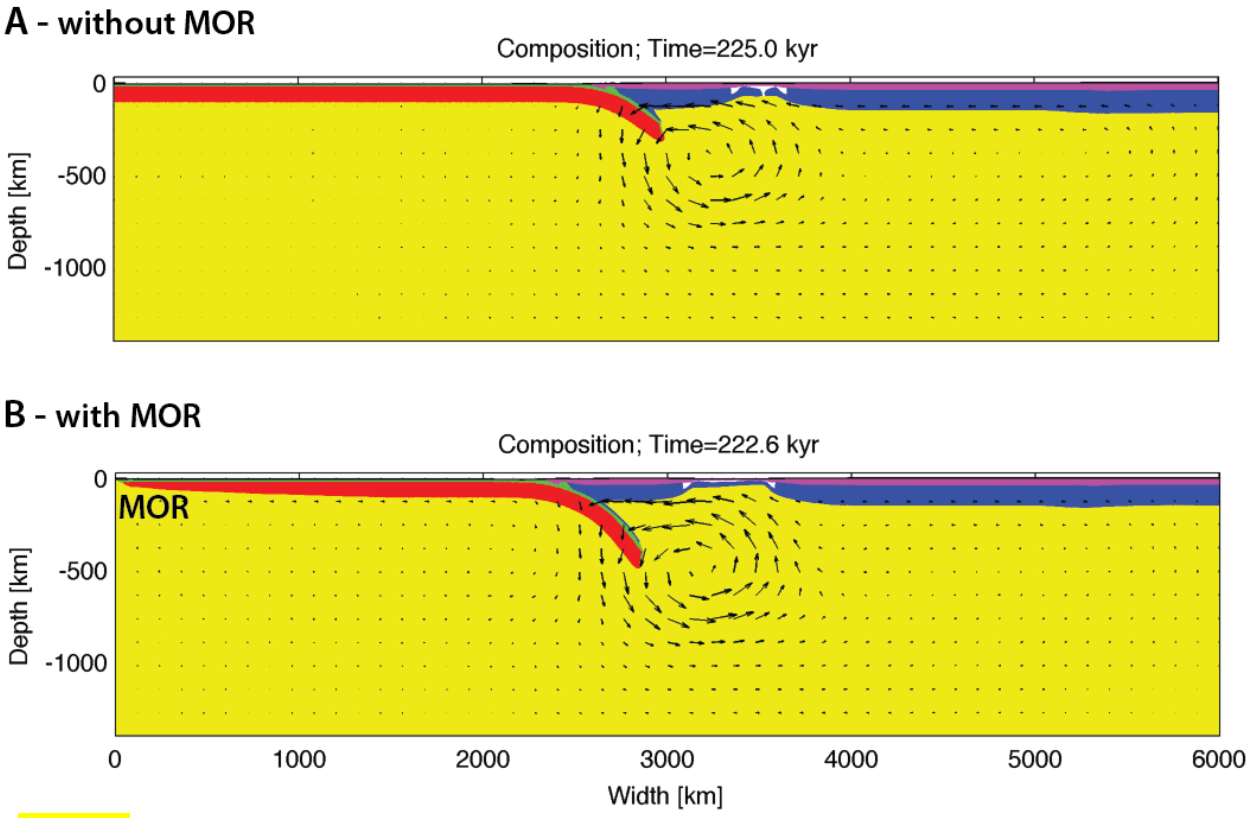

329
330 *Figure 4. Results of two simulations to compare subduction initiation in an ocean without (A –*

Model 1) and with (B – Model 2) a mid-ocean rift (MOR). The only difference in the initial setup between the two models was the temperature profile in the oceanic lithosphere. Note that subduction initiated faster when there was a MOR.

Model 1

Given the objectives that we defined for these simulations, we only present one result for comparison with Model 2 (Fig. 4). Despite the only difference in the initial setup between the two models being the temperature profile in the oceanic lithosphere, subduction initiated significantly faster in the model with a MOR. From these results we infer that ridge-push added to the other topographic forces to make subduction initiation faster.

Model 2

The most relevant results of Model 2 are shown in Figs. 5 and 6. Very early in the numerical experiments (Fig. 5b), the model deep Andean roots rose isostatically, the topography started to decrease (Fig. 6b), and the continent thrust over the ocean. Continental thrusting over ocean, by spreading of the model Andes and rise of its roots, was soon followed by subduction initiation (Fig. 5c), which comprised slab rollback and consequent trench retreat. The fast sinking slab induced fast trench retreat, which overcame the opposing overthrusting velocity to produce extension in the continental overriding plate and open a back-arc basin at the lithospheric weakness (Figs. 5 and 6b, c). After ca. 850 kyr (Fig. 5d) the trench had already retreated ca. 830 km, and the back-arc basin had already opened ca. 750 km. At ca. 850 ky, the topography had already decreased to less than 2 km altitude by collapse of the model Andean Plateau.

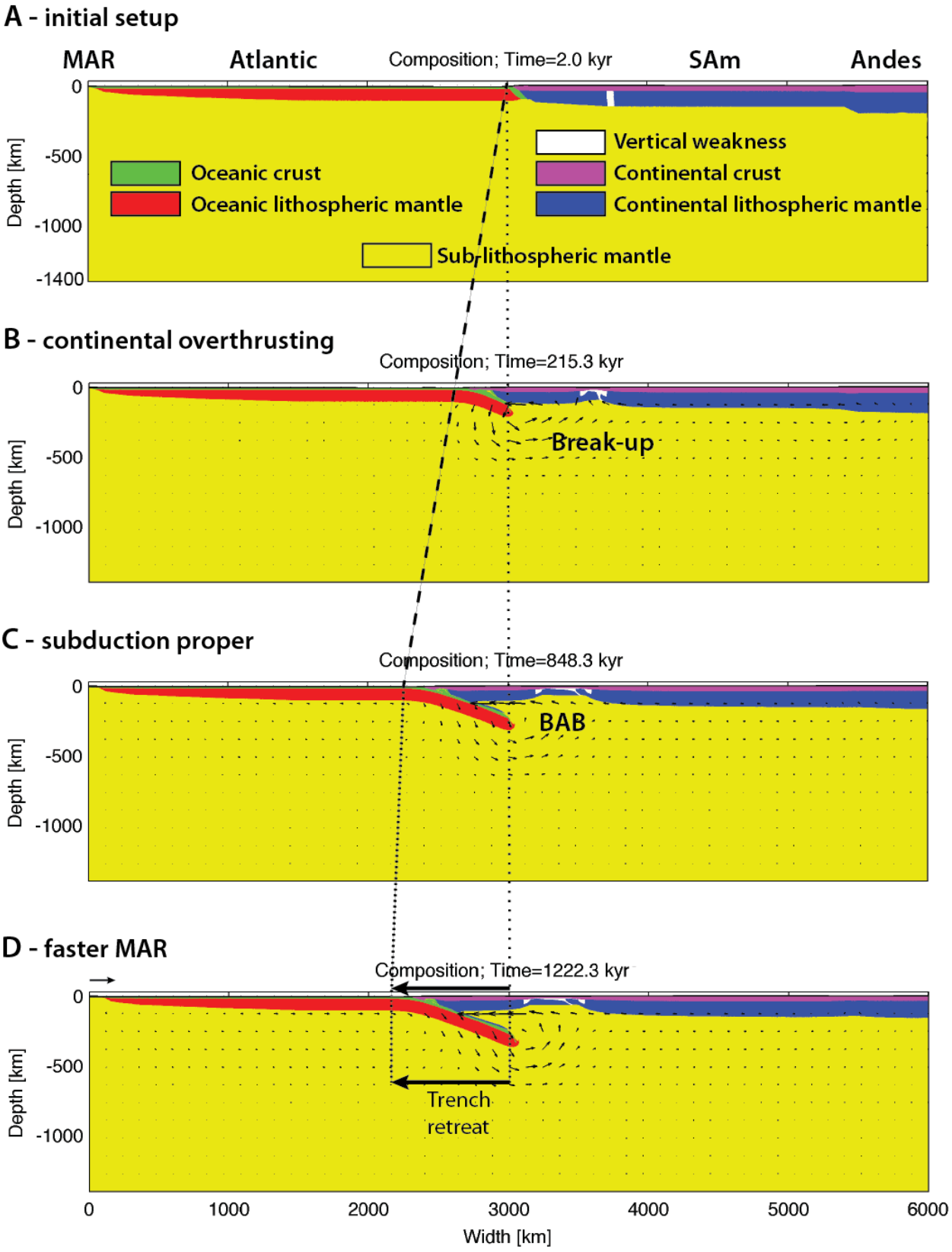

354

355 *Figure 5. A to D are images of Model 2 at different time steps, showing: (A) initial setup; (B)*

356 *early continental overthrusting, trench retreat and break-up in the overriding SAm; (C)*

357 *subduction proper, and consequent opening of back-arc basin (BAB); and (D) beginning of*

slow-down in trench retreat due to faster spreading in the MAR, as shown by different slopes in dashed and dotted lines (cf. graph in Fig. 8). Note that the initial deep Andean roots rose and almost vanished before 1 Ma.

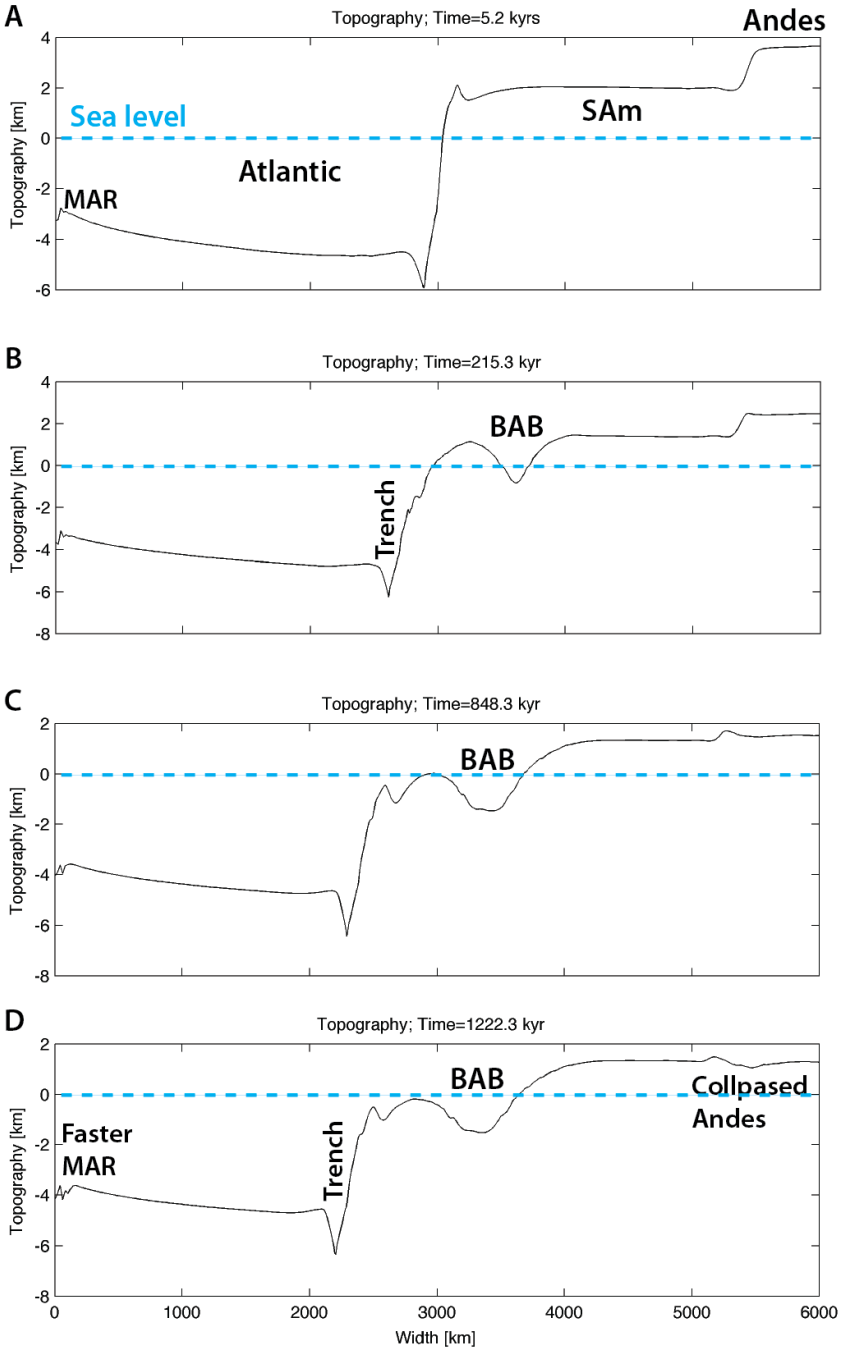

Figure 6. Images depicting the topographic evolution in Model 2. In the initial stage (A) there is a model Andean Plateau at ca. 4 km height (as in the Andes), which decreases altitude by gradual collapse and horizontal spreading (B, C), until less than 2 km altitude before 1 Ma (C). Spreading of the model SAm produces thrusting of continent over ocean, and ultimately

subduction initiation with development of a deep trench (B). Self-sustained subduction includes rollback, which produces trench retreat and a back-arc basin (BAB) (C, D). Vertical scale exaggerated 330 x for a clear view of the topography.

In the beginning, the collapse of the Andes induces thrusting of continent over ocean at the margin, therefore the whole continent is under compression (Fig. 5a). When subduction initiates, the trench retreats, and at a certain time step trench velocity overcomes continental spreading and a back-arc starts to form (this can be more clearly seen in the supplementary videos). At this stage, the force balance shown in Fig. 3 is changed, and the back-arc basin widens (Fig. 5c).

Given that the position of the rift did not change until ca. 1 Ma (Fig. 5c, d), we infer that slab-pull was not enough to drag the oceanic lithosphere over the underlying mantle. Therefore, trench retreat was fast. Conversely, after ca. 1 Ma the MOR was spreading (Fig. 5d), which means that the oceanic lithosphere was sliding over the mantle and, therefore, trench retreat slowed down to the lowest velocities.

The temperature map (Fig. 7a) shows the initial temperature profile, including the typical oceanic profile wedging out toward the MOR, and the temperature evolution after ca. 850 ky. Noticeable at this stage is the cold slab in a hot mantle due to thermal disequilibrium between slab (colder by fast advection of low temperatures to depth with small thermal re-equilibration with host mantle) and host mantle (hotter). The great temperature contrast between slab (cold and therefore denser, as shown in Fig. 7b) and host mantle was in great part responsible for the fast subduction. The temperature profile at ca. 850 ky also shows a hot back-arc basin, with sharp contacts between hot rising mantle and cold continental lithosphere.

The stress map (Fig. 7b) shows stress concentration in the oceanic lithosphere in the early stages, gradually increasing from the MOR towards the contact with the continental lithosphere.

391 On the continental side, stresses concentrated mostly close to the weak zones, i.e. the Andean
392 roots, the ocean/continent contact, and the lithospheric vertical weakness. Later on, stresses
393 concentrated mostly in the sinking slab, and between the Andes and the newly formed back-arc

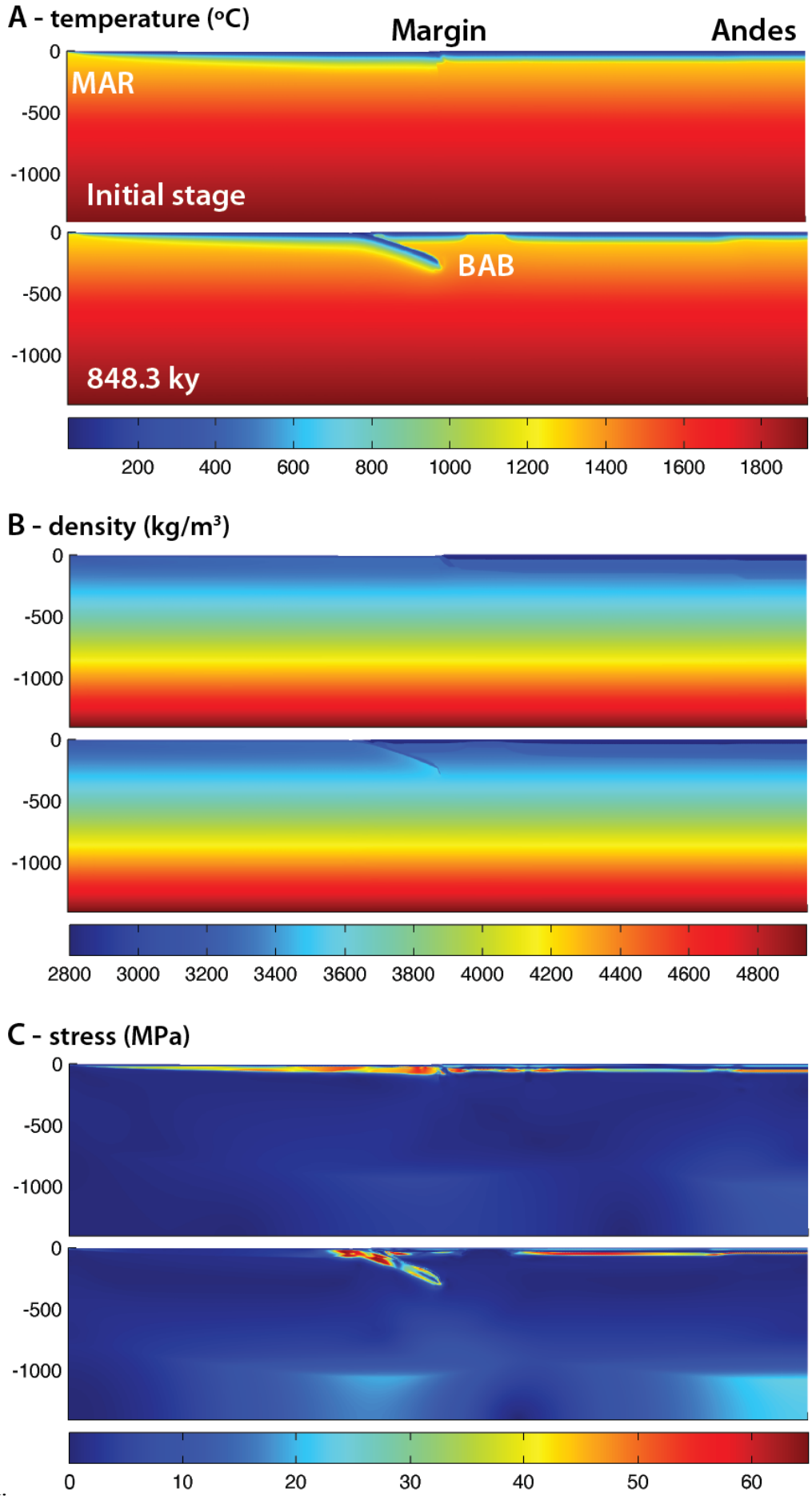
A - temperature (°C)
Margin
Andes
MAR
Initial stage
BAB
848.3 ky
0
-500
-1000
200 400 600 800 1000 1200 1400 1600 1800
B - density (kg/m³)
2800 3000 3200 3400 3600 3800 4000 4200 4400 4600 4800
C - stress (MPa)
0 10 20 30 40 50 60

394 basin.

Figure 7. Results of a simulation to show the distribution of temperature (A), density (B) and stress (C) in the model, in the initial stage (top panel of each pair) and after ca. 850 ky (bottom panel of each pair). Note the cold sinking slab, and the stress concentration in the oceanic lithosphere, especially towards the contact with the continental lithosphere, and, later on, also in the sinking slab.

We also analysed the variation of subduction and trench velocities over time (Fig. 8). The presented graphs show that the two velocities have a power-law dependence on time, and very similar trends. However, the subduction velocity, especially in the early stages, is higher than the trench velocity. Given that the oceanic plate did not slide over the mantle in the early stages of subduction, the difference in velocities means that not all subducted oceanic lithosphere was directly transformed into trench retreat. Later on (Fig. 5d and supplementary video), slab-pull was enough to drag the oceanic plate toward the trench and induce opening at the MOR. This means that until ca. 850 ky the absolute horizontal velocity of the oceanic plate was zero, and later there was an absolute horizontal velocity toward the west.

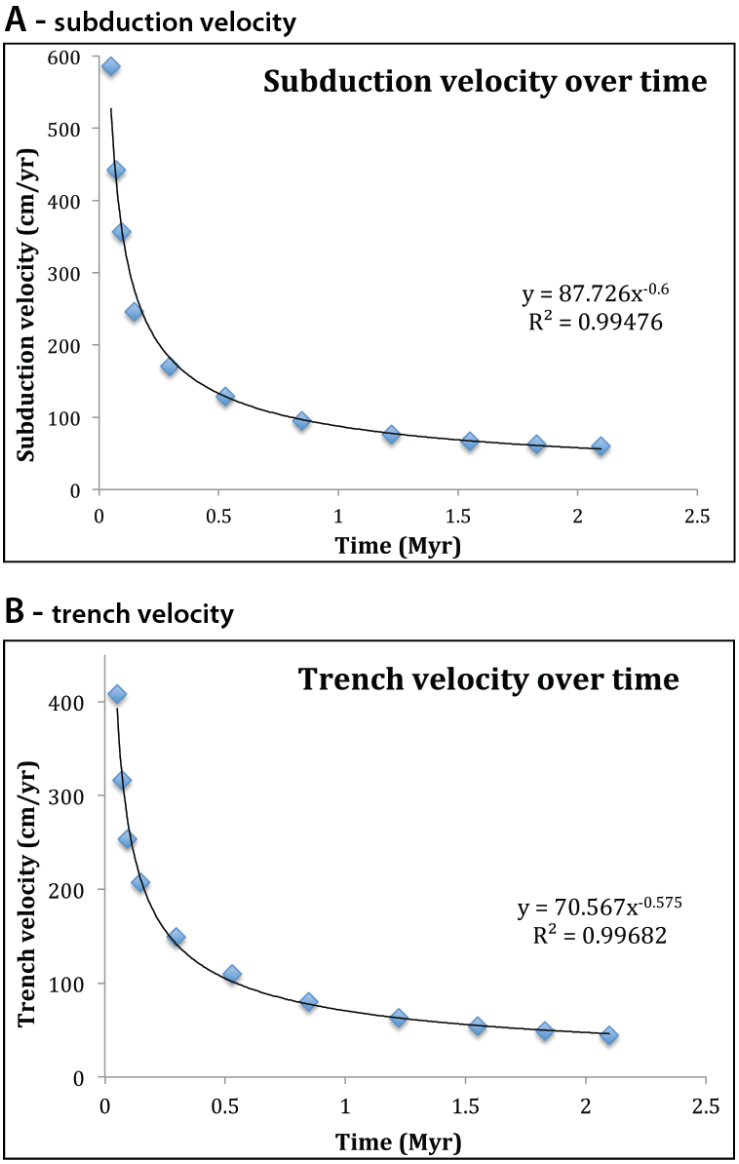

Figure 8. Graphs representing the variation of subduction (A) and trench (B) velocities over time.

Given the persisting uncertainties regarding the rheology of the upper mantle, we decided to analyse the effects of linear or power-law rheology on subduction initiation (e.g. Billen and Hirth, 2005, 2007). We made three different simulations (Fig. 9), differing only on the creep law: one with dislocation creep (power-law), one with diffusion creep (linear viscous), and one in which we prescribe both dislocation and diffusion, and the code decides which to use based on the other parameters in the constitutive equations. From the model results two main points stand

out: (1) diffusion creep hampers subduction initiation, similarly to the simulations reported in Billen and Hirth (2005). With prescribed diffusion creep (Fig. 9c), there was mostly continental overthrusting, not actual subduction, after more than 20 Ma. (2) The results in Fig. 9a (prescribed dislocation creep) and Fig. 9b (prescribed dislocation and diffusion creeps) are indistinguishable, which means that the model in Fig. 9b chose dislocation creep.

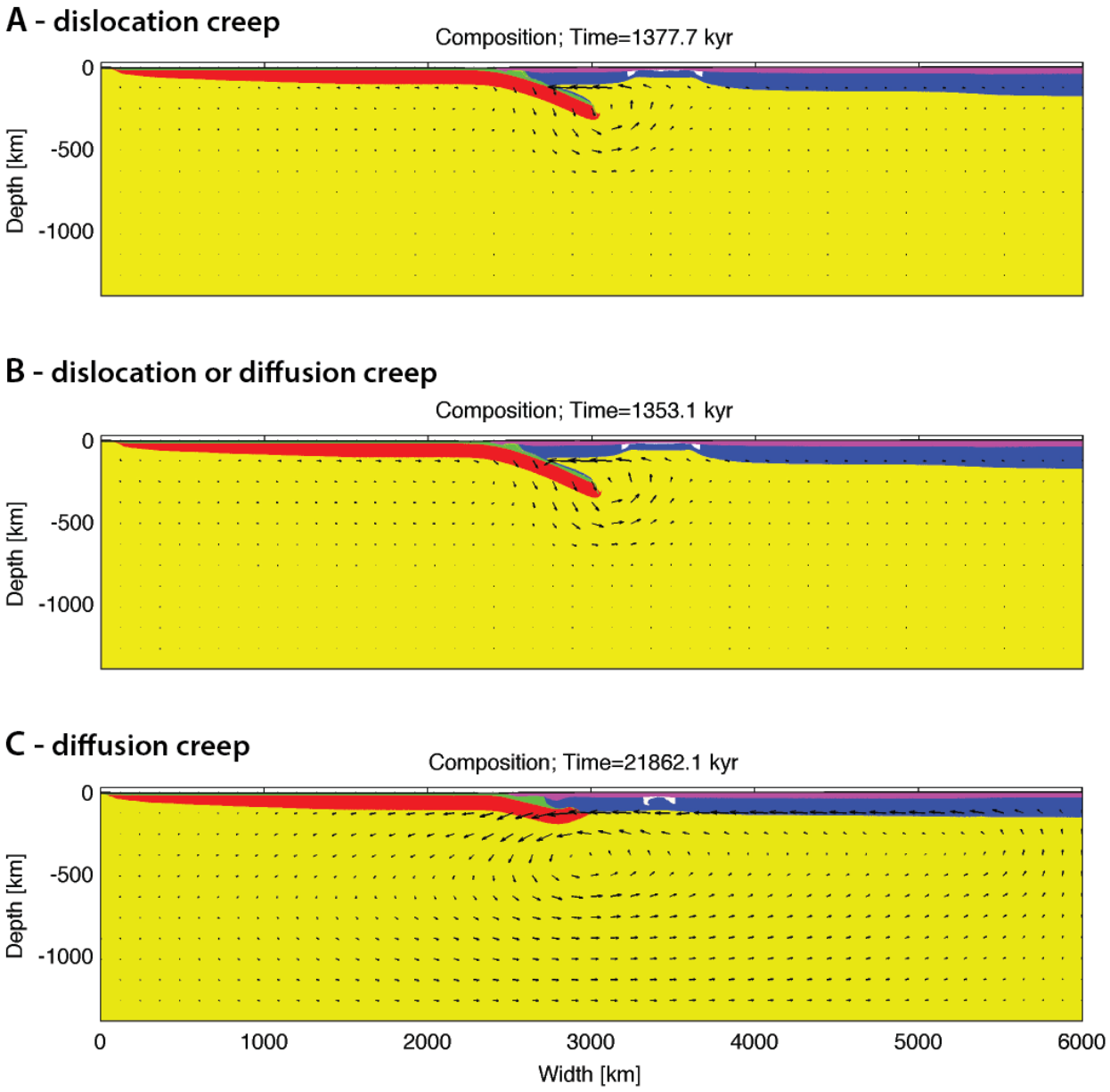

Figure 9. Results of three simulations in which the only difference is that in (A) we prescribed dislocation creep, in (B) we made dislocation and diffusion creeps optional, and in (C) we

prescribed diffusion creep. Note that the results in A and B are indistinguishable, which means that the model in (B) chose dislocation creep. Also note that, with prescribed diffusion creep (C), after more than 22 Ma there was mostly continental overthrusting, not actual subduction.

Knowing that the experimentally derived values of the activation volume (V) vary in a wide range (13±8 cm^3/mol according to the statistical analysis of Korenaga and Karato, 2008), we analysed the effects of V on the velocities of subduction and trench (Fig. 10). The graphs show an exponential dependence of velocity on V, and little difference between the subduction and trench velocities. This means that, for the analysed age, practically all sunken slab length corresponded to trench retreat, as forecasted in Fig. 1.

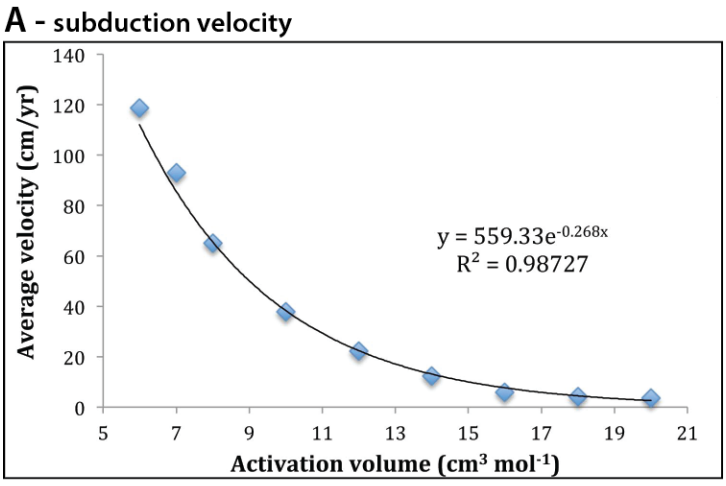

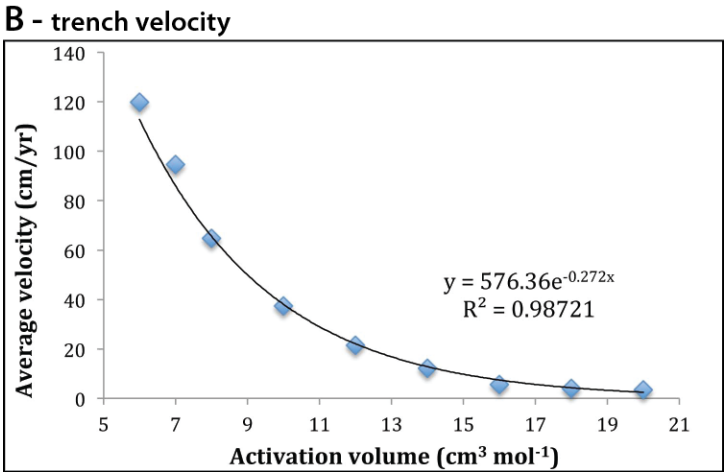

Figure 10. Graphs to show the effects of activation volume (V) on the velocities of subduction (A) and trench (B). Note the small difference between the two velocities.

Model 3

This model is an extension of Model 2 to encompass a full ocean with a MOR (model of Atlantic with the MAR) and the continent on the opposite side of the ocean (model Africa). We limit ourselves to presenting Fig. 11 (and supplementary video 2) with the most representative time steps for comparison with Model 2 in Fig. 5.

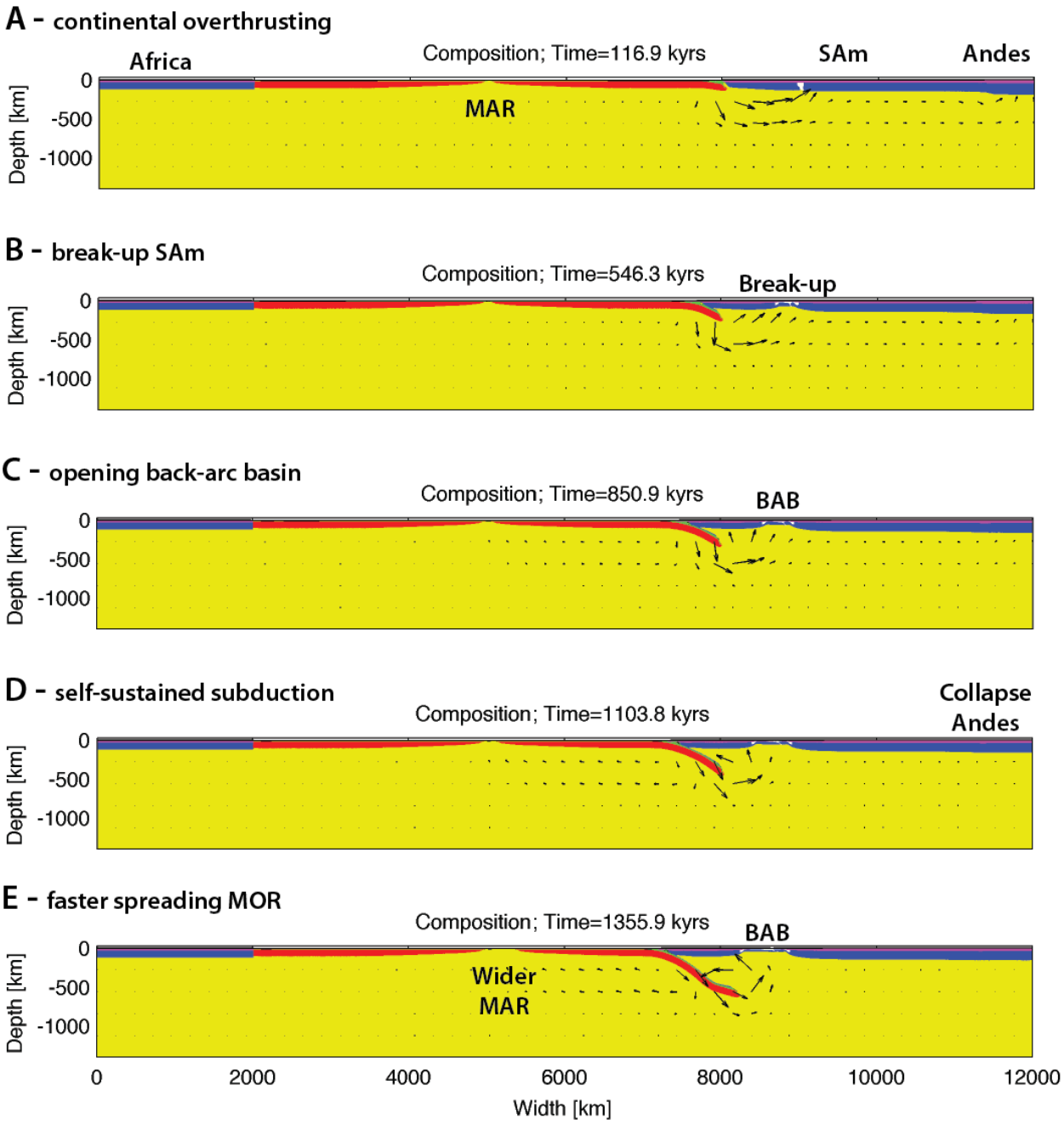

449

450 *Figure 11. A to D are images of Model 3 at different time steps, showing: (A) early continental*
451 *overthrusting; (B) trench retreat and break-up in the overriding SAm; (C) subduction proper,*
452 *and consequent opening of back-arc basin (BAB); (D) self-sustained subduction; and (E)*
453 *beginning of slow-down in trench retreat due to faster spreading in the MAR. Note that the*
454 *initial deep Andean roots rose and almost vanished before 1 Ma.*

455

456 **4. Future evolution of the South American Plate**

When the SAm breaks up along the Atlantic passive margin to initiate subduction, the force balance depicted in Fig. 3 will change significantly, because two new plates will form that were previously welded together and now move independently: the continental SAm (CSAm) and the oceanic SAm (OSAm). Once subduction has initiated, a major geodynamic reconfiguration of the SAm will take place, because the stresses will shift from compressive (cf. Fig. 3) to tensile on the continental SAm, as well illustrated by the numerical modelling with the opening of a back-arc basin.

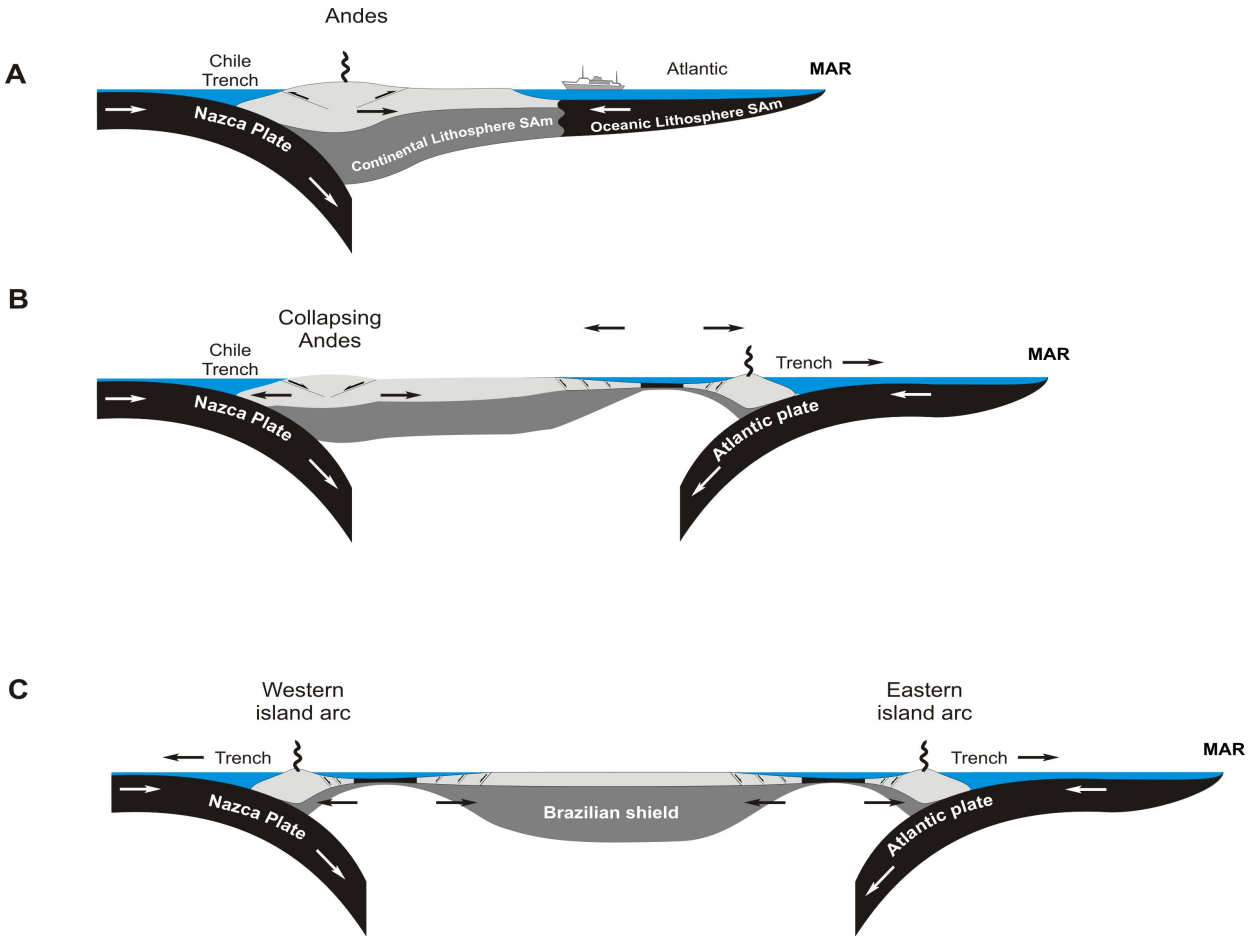

Figure 12. Sketch of forecasted evolution stages, in W-E sections, after subduction initiation at the Brazilian passive margin. A – current tectonic setting. B – subduction initiation at the Brazilian margin will induce, by trench retreat, formation of an island arc and a back-arc basin in the overriding plate. The Andes will collapse because the present compressive

stresses will invert to tensile, and thus lose support. A new island arc will form with a back-arc basin. C – final stage after a few millions of years, in which the Andes are replaced by an island arc with a back-arc basin, similarly to the setting 150 Ma ago with a back-arc basin known as the Neuquén Basin. Full arrows represent velocities, and half arrows indicate fault kinematics.

The ridge push from the east (MAR push) will no longer affect the CSAm, because the current Atlantic margin will become a trench (Figs. 3, 12b, 13) and ridge-push will add positively to the newly born slab-pull and promote fast subduction similarly to the presented simulations (Figs. 4 and 5d). If subduction initiation is accompanied by subduction roll-back and trench retreat, as indicated by previous and here presented models (Figs. 4 and 5), the continental SAm will be under extension, instead of the current compression. Given that the subduction roll-forth (compression due to trench advance) in the west (Nazca Plate) is just relative (e.g. Russo and Silver, 1996, in particular their Fig. 3), the trench motion will go back to absolute trench retreat to the west, so inducing extension in the overriding SAm, because the westward velocity of South America will flip to eastward velocity. Without buttressing from east (ridge push) and west (relative roll-forth)(Fig. 3), the Andes will collapse (Figs. 5, 6 and 12b, c). The sinking of the new subducting Atlantic slab, and associated rollback subduction and trench retreat (Figs. 5, 6 and 12b), will drive extension in the overriding plate with formation of an island arc (like the Japanese), with a back-arc basin (like the Sea of Japan). If an oceanic rift initiates in the back-arc, then a new plate will form comprised of the new island arc.

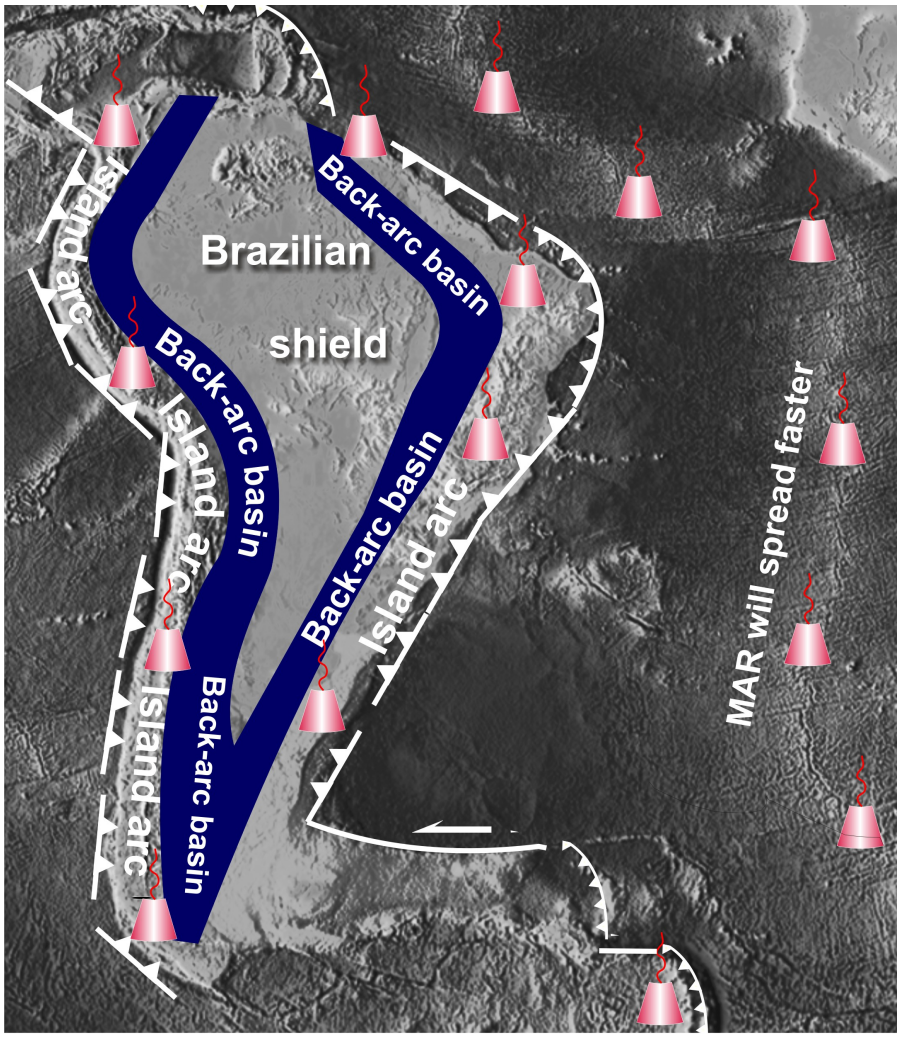

Figure 13. Forecasted scenario for the reconfiguration of the South American plate. Background image is a shaded relief image from ETOPO5 digital data (http://www.ngdc.noaa.gov/mgg/global/relief/etopo5/images/tif/slides_t/slide15.tif).

The new slab pull associated with the sinking Atlantic lithosphere will add positively to the MAR push (similarly to the East Pacific Rise where full spreading rates can amount to 120 mm/yr), and therefore increase the MAR spreading rate substantially (presently only ca. 30 mm/yr), similarly to what we observed in the numerical simulations (Fig. 5d, and supplementary videos). Then, the shape of the MAR will also change, especially by increasing its volume (similarly to the East Pacific Rise). The CSAm's velocity will flip from westward to eastward directed, due to new eastward trench suction in the east, and loss of westwards MAR push.

Without the westward CSAm's velocity, the relative roll-forth of the Nazca plate will become absolute rollback (Russo and Silver, 1996), and the push of the hinge roll-forth on the western boundary of the CSAm will vanish and invert to trench suction. With pull from the east and west (trench suction, opposite to current push), the Andes will completely collapse (Figs. 6 and 12b, c). Due to Nazca absolute rollback, an island arc will form in western CSAm, with a back-arc basin separating the new island arc from the CSAm (Fig. 12c), similarly to what has already happened in the past with the opening of the Neuquén Basin (cf. Fig. 3 in Russo and Silver, 1996). If an oceanic rift initiates in the back-arc, then a new tectonic plate will form comprised of the new island arc. Rifting along the E and W boundaries of the SAm will isolate the old, thick and resistant Brazilian shield, which will then comprise a new tectonic plate (Figs. 12c, and 13).

One can argue that the velocities in our models are too high, and question if such fast rates are reasonable or not in the Earth; that models have limitations, and how the model results compare with previous work and observations in nature; that there are no known natural counterparts in the current known subduction velocities, and we should validate the numerical results with natural examples; that the Andes could be supported by mantle drag so preventing collapse; and that the three-dimensional nature of the prototype is not taken into account in our 2-dimensional models. In the following we discuss these questions.

First of all, we recall the reader that the objective of this study is the catastrophic end-member of subduction initiation, which is the one capable of producing catastrophic consequences in the Earth system. Having made this point clear, the main question is if such fast rates are reasonable or not in the Earth. There is only one answer to this question: yes, if we use the current knowledge of Earth's rheology through the experimentally deduced constitutive equations and experimentally determined parameters. This is what we did in our models; using well-known equations and conservative values of the parameters that are still less well

established, we show that subduction can initiate very fast. In fact, previous models (cf. Fig. 6 of Nikolaeva et al., 2010) showed that the velocities of subduction initiation can be of the order of the ones now obtained in our models. We just tested different parameters. Moreover, we also tested the effects of diffusion and dislocation creeps, and the models show that under the used setup the code chose dislocation creep.

Regarding mantle drag, the current knowledge about the SAm has shown that the stresses born from topography gradients in the SAm are propagated throughout the SAm (e.g. Coblentz and Richardson, 1996), which means that the mantle is not resistive to the point of preventing stresses to propagate through the entire plate. Moreover, it goes against all evidence of current deformation along the SAm's Atlantic continental margin and interior Brazil (e.g. Bezerra and Vita-Finzi, 2000; Marques et al., 2014; Nogueira et al., 2015; Cogné et al., 2001, 2012, 2013). If mantle drag could support the Andes, then the forces available to initiate subduction at the Brazilian margin would most likely be insufficient to initiate subduction (Nikolaeva et al., 2011). Based on the current knowledge of stress distribution in the SAm, one main premise of our modelling is that the Andes push the entire SAm lithosphere to the east, thus being able to trigger subduction initiation at the Brazilian margin. This is also what our models show. With well-known constitutive equations and reasonable parameters used by geodynamic modellers, mantle drag exists in our models but not to the point of preventing Andean collapse and propagation of the stresses to the Brazilian margin, with consequent subduction initiation.

The remaining questions have no straightforward answer. Our models cannot be directly compared with previous models, because our models were fully gravitational (which is not the case of most previous models, in which velocities are prescribed at the boundaries and therefore do not reflect natural gravitational forces), incorporated the effects of topographical forcing (only comparable to Nikolaeva et al., 2011; Marques et al., 2013), and had a pressure-dependent density (which does not exist in analogue modelling and has not been used in numerical

553 modelling). We cannot compare simulated subduction initiation with present-day subduction,
554 because everywhere in the Earth subduction is mature, and nowhere is at the early stage of
555 subduction initiation that we analyse in our models. We are aware of the three-dimensional
556 effects on subduction initiation (Marques et al., 2014). These authors showed that the curvature
557 of a passive margin can influence the timing of subduction initiation, but this does not mean that
558 subduction will not initiate.

559 Finally, the argument that the model has not been validated by natural examples is
560 misleading, because: (1) the "*Absence of evidence is not evidence of absence*". (2) To our
561 knowledge, there is no known record of the very early stages of subduction initiation at a passive
562 margin of Atlantic type, even in the Cainozoic (e.g. Stern, 2004); therefore we cannot compare
563 our models with nature. Subduction initiation in the Bay of Biscay (e.g. Le Pichon and Sibuet,
564 1971; Boillot et al., 1979; Alvarez-Marrón et al., 1996; Alvarez-Marrón et al., 1997) underwent
565 only the first stage as defined by Nikolaeva et al. (2010), which is thrusting of continental Iberia
566 over oceanic Bay of Biscay. However, the statement there is no known record of the very early
567 stages of subduction initiation at a passive margin of Atlantic type does not mean that it does
568 exist. It means that it has so far not been found. Our hope is that the present study, based on well-
569 established Physics, although speculative about the consequences, motivates geologists to go and
570 look for the missing evidence.

571

572 **5. Impact on the Earth system**

573 The Andean cordillera stretches north south for ca. 7,000 km, it includes the impressive
574 Altiplano-Puna Plateau with an average altitude of ca. 4 km, and it spreads most types of climate.
575 If we accept that the Andean cordillera is a first order control of atmospheric circulation (Insel et
576 al., 2010), then its collapse will produce significant changes in atmospheric circulation, and thus
577 drive climate change. If our predictions are correct, then SAm's reconfiguration will include the

opening of large-scale oceanic circulation between the Pacific and the Atlantic, currently restricted to SAm's southern end. Once the new oceanic circulation initiates, it will have a significant impact on the thermohaline circulation, whose large heat transport makes it critical for atmospheric circulation, and therefore climate change (Manabe and Stouffer, 1993; Rahmstorf, 1997; Stocker and Schmittner, 1997; Clark, et al., 2002; Rahmstorf, 2002).

Two new island arcs (and possibly two new rifts) and a much faster spreading MAR, each able to reach 5 to 7,000 km length, might throw significant amounts of greenhouse and toxic gases into the hydrosphere and atmosphere, whose effects on climate change (Cox et al., 2013; Cox et al., 2008; Lewis et al., 2009; Malhi et al., 2008) and biotic crisis have been extensively discussed (Kennett and Stott, 1991; MacLeod and Huber, 1996; Wignall and Twitchett, 1996; Wignall, 2001; Grasby et al., 2011; Song et al., 2013; Richoz et al., 2012). The great reconfigurations of SAm and MAR might produce sea-level changes, but this is very difficult to evaluate because there seem to be opposing effects, like the increase in volume of the faster spreading MAR (sea-level rise), and the opening of new seas/oceans (sea-level drop). Anyway, sea level changes are a major concern, and can be produced by variations in the ice caps by climate change (Miles et al., 2013; Hanna et al., 2013). If subduction initiation along the Atlantic SAm propagates to the North American Atlantic margin (complete reconfiguration of the South and North American tectonic plates), then the impact of subduction initiation on global changes can be even much greater. If it is true that flood basalts can be responsible for great mass extinctions in 1 Ma (Duncan and Pyle, 1988; Courtillot et al., 1988), then the geodynamic reconfigurations here forecasted will produce dramatic global changes, because the scale of transformations associated with the subduction initiation process is many orders of magnitude greater. A comparison cannot be made with the impact human activity may have on climate change, but scenarios have been proposed that include natural and anthropogenic causes (Moss et al., 2010).

603 To conclude, the substantially increased volcanism all around the South American Plate
604 and in the MAR might release large amounts of greenhouse and toxic gases into the atmosphere
605 and oceans, and the plate reconfiguration will lead to major oceanic and atmospheric circulation
606 changes. Ultimately, these large-scale transformations will trigger global changes and impact the
607 whole Earth system.
608
609 **References**
610 Alvarez-Marrón, J., et al., 1996. Seismic structure of the northern continental margin of Spain
611 from ESCIN deep seismic profiles. Tectonophysics 264, 355-363.
612 Alvarez-Marrón, J., Rubio, E., Torne, M., 1997. Subduction-related structures in the North
613 Iberian Margin. J. Geophys. Res. 102, 2497-2511.
614 Artemieva, I.M., Mooney, W.D., 2001. Thermal thickness and evolution of Precambrian
615 lithosphere: A global study. Journal of Geophysical Research 106, 16,387–16,414.
616 Artyushkov, E.V., 1987. The forces driving plate motions and compression of the crust in fold
617 belts. In: Composition, Structure and Dynamics of the Lithosphere-Asthenosphere System.
618 Fuchs, K., Froidevaux, C. (Eds.). Geodynamics Series 16, 175-188, AGU.
619 Assumpção, M., 1992. The regional intraplate stress field in South America. Journal of
620 Geophysical Research 97, 11889-11903.
621 Bercovici, D., Long, M.D., 2014. Slab rollback instability and supercontinent dispersal,
622 Geophys. Res. Lett. 41, doi:10.1002/2014GL061251.
623 Bezerra, F.H.R., Vita-Finzi, C., 2000. How active is a passive margin? Paleoseismicity in
624 northeastern Brazil. Geology 28, 591-594.
625 Billen, M.I., Hirth, G., 2005. Newtonian versus non-Newtonian upper mantle viscosity:
626 Implications for subduction initiation. Geophys. Res. Lett. 32, L19304.
627 Billen, M.I., Hirth, G., 2007. Rheologic controls on slab dynamics. Geochem. Geophys. Geosyst.

628 8, Q08012.
629 Boillot, G., Dupeuble, P.A., Malod, J., 1979. Subduction and tectonics on the continental margin
630 off northern Spain. Mar. Geol. 32, 53-70.
631 Bürgmann, R., Dresen, G., 2008. Rheology of the Lower Crust and Upper Mantle: Evidence
632 from Rock Mechanics, Geodesy, and Field Observations. Ann. Rev. Earth Planet. Sci. 36,
633 531-567.
634 Capitanio, F.A., Stegman, D.R., Moresi, L.N., Sharples, W., 2010. Upper plate controls on deep
635 subduction, trench migrations and deformations at convergent margins. Tectonophysics 483,
636 80–92.
637 Clark, P.U. et al., 2002. The role of the thermohaline circulation in abrupt climate change.
638 Nature 415, 863−869.
639 Coblentz, D.D., Richardson, R.M., 1996. Analysis of the South American intraplate stress field.
640 Journal of Geophysical Research 101, 8643-8657.
641 Cogné, N., Cobbold, P.R., Riccomini, C., Gallagher, K., 2013. Tectonic setting of the Taubaté
642 Basin (southeastern Brazil): Insights from regional seismic profiles and outcrop data. J. South
643 Am. Earth Sci. 42, 194-204.
644 Cogné, N., Gallagher, K., Cobbold, P.R., 2011. Post-rift reactivation of the onshore margin of
645 southeast Brazil: Evidence from apatite (U-Th)/He and fission-track data. Earth Planet. Sci.
646 Lett. 309, 118-130.
647 Cogné, N., Gallagher, K., Cobbold, P.R., Riccomini, C., Gautheron, C., 2012. Post-breakup
648 tectonics in southeast Brazil from thermochronological data and combined inverse-forward
649 thermal history modelling. Journal of Geophysical Research 117, B11413,
650 doi:10.1029/2012JB009340.
651 Courtillot, V., Feraud, G., Maluski, H., Vandamme, D., Moreau, M.G., Besse, J., 1988. Deccan
652 flood basalts and the Cretaceous/Tertiary boundary. Nature 333, 843-846.

653 Cox, P.M. et al., 2008. Increasing risk of Amazonian drought due to decreasing aerosol
654 pollution. Nature 453, 212–215.
655 Cox, P. M. et al., 2013. Sensitivity of tropical carbon to climate change constrained by carbon
656 dioxide variability. Nature 494, 341–344.
657 Crameri, F., Kaus, B., 2010. Parameters that control lithospheric-scale thermal localization on
658 terrestrial planets. Geophys. Res. Lett. 37, L09308.
659 Crameri, F. et al., 2012. A comparison of numerical surface topography calculations in
660 geodynamic modelling: an evaluation of the 'sticky air' method. Geophys. J. Int. 189, 38–54.
661 Dabrowski, M., Krotkiewski, M., Schmid, D.W., 2008. MILAMIN: MATLAB-based finite
662 element method solver for large problems. Geochemistry, Geophysics, Geosystems 9,
663 Q04030.
664 Di Giuseppe, E., Faccenna, C., Funiciello, F., van Hunen, J., Giardini, D., 2009. On the relation
665 between trench migration, seafloor age, and the strength of the subducting lithosphere.
666 Lithosphere 1, 121–128.
667 Di Giuseppe, E., van Hunen, J., Funiciello, F., Faccenna, C., Giardini, D., 2008. Slab stiffness
668 control of trench motion: Insights from numerical models. Geochem. Geophys. Geosys. 9,
669 Q02014.
670 Duncan, R.A., Pyle, D.G., 1988. Rapid eruption of the Deccan flood basalts at the
671 Cretaceous/Tertiary boundary. Nature 333, 841-843.
672 Elsasser, W.M., 1971. Sea-floor spreading as thermal convection. Journal of Geophysical
673 Research 76, 1101–1112.
674 Faccenna, C., Giardini, D., Davy, P., Argentieri, A., 1999. Initiation of subduction at Atlantic
675 type margins: insights from laboratory experiments. J. Geophys. Res. 104, 2749–2766.
676 Feng, M., van der Lee, S., Assumpção, M., 2007. Upper mantle structure of South America from
677 joint inversion of waveforms and fundamental mode group velocities of Rayleigh waves.

678 Journal of Geophysical Research 112, B04312, doi: 10.1029/2006JB004449.
679 Forsyth, D.W., Uyeda, S., 1975. On the relative importance of the driving forces of plate motion.
680 The Geophysical Journal of the Royal Astronomical Society 43, 163–200.
681 Funiciello, F., Faccenna, C., Giardini, D., Regenauer-Lieb, K., 2003a. Dynamics of retreating
682 slabs: 2. Insights from three-dimensional laboratory experiments. Journal of Geophysical
683 Research 108 (B4), 2207. doi:10.1029/2001JB000896.
684 Funiciello, F., Faccenna, C., Heuret, A., Lallemand, S., Giuseppe, E.D., Becker, T.W., 2008.
685 Trench migration, net rotation and slab-mantle coupling. Earth Planet. Sci. Lett. 271, 233-
686 240.
687 Funiciello, F., Moroni, M., Piromallo, C., Faccenna, C., Cenedese, A., Bui, H.A., 2006. Mapping
688 mantle flow during retreating subduction: laboratory models analyzed by feature tracking.
689 Journal of Geophysical Research 111, B03402. doi:10.1029/2005JB003792.
690 Funiciello, F., G. Morra, K. Regenauer-Lieb, D. Giardini, 2003b. Dynamics of retreating slabs:
691 1. Insights from two-dimensional numerical experiments, J. Geophys. Res. 108, 2206,
692 doi:10.1029/2001JB000898.
693 Gerya, T.V., Yuen, D.A., 2007. Robust characteristics method for modelling multiphase visco-
694 elasto-plastic thermo-mechanical problems. Phys. Earth Planet. Int. 163, 83–105.
695 Grasby, S. E., Sanei, H., Beauchamp, B., 2011. Catastrophic dispersion of coal fly ash into
696 oceans during the latest Permian extinction. Nature Geosci. 4, 104–107.
697 Gurgel, S.P.P., Bezerra, F.H.R., Corrêa, A.C.B., Marques, F.O., Maia, R.P., 2013. Cenozoic
698 uplift and erosion of structural landforms in NE Brazil. Geomorphology 186, 68-84.
699 Gurnis, M., Hall, C., Lavier, L., 2004. Evolving force balance during incipient subduction.
700 Geochem. Geophys. Geosyst. 5, Q07001, doi:10.1029/2003GC000681.
701 Gvirtzman, Z., Nur, A., 1999. The formation of Mount Etna as the consequence of slab rollback.
702 Nature 401, 782−785.

Hall, C.E., Gurnis, M., Sdrolias, M., Lavier, L.L., 2003. Catastrophic initiation of subduction following forced convergence across fracture zones. Earth and Planetary Science Letters 212, 15–30.

Heit, B., Sodoudi, F., Yuan, X., Bianchi, M., Kind, R., 2007. An S receiver function analysis of the lithospheric structure in South America. Geophys. Res. Lett. 34, L14307, doi:10.1029/2007GL030317.

Hirth, G., Kohlstedt, D., 2003. Rheology of the upper mantle and the mantle wedge: A view from the experimentalists. In J. Eiler (ed) Inside the Subduction Factory, Geophysical Monograph American Geophysical Union, Washington, D.C. 138, 83–105.

Holt, A., Becker, T.W., Buffett, B.A., 2015. Trench migration and overriding plate stress in dynamic subduction models. Geophys. J. Int. 201, 172–192, doi:10.1093/gji/ggv011.

Husson, L., Conrad, C.P., Faccenna, C., 2008. Tethyan closure, Andean orogeny, and westward drift of the Pacific Basin. Earth Planet. Sci. Lett. 271, 303-310.

Insel, N., Poulsen, C.J., Ehlers, T.A., 2010. Influence of the Andes Mountains on South American moisture transport, convection, and precipitation. Climate Dynamics 35, 1477−1492.

Johnson, T.E., Brown, M., Kaus B.J.P., Van Tongeren, J.A., 2014. Delamination and recycling of Archean crust caused by gravitational instabilities. Nature Geoscience 7, 47-52.

Karato, S.-I., Wu, P., 1993. Rheology of the Upper Mantle: A Synthesis. Science 260, 771-778.

Kaus, B., 2010. Factors that control the angle of shear bands in geodynamic numerical models of brittle deformation. Tectonophysics 484, 36–47.

Kennett, J.P., Stott, L.D., 1991. Abrupt deep-sea warming, palaeoceanographic changes and benthic extinctions at the end of the Palaeocene. Nature 353, 225−229.

Kincaid, C., Griffiths, R.W., 2003. Laboratory models of the thermal evolution of the mantle during rollback subduction. Nature 425, 58–62.

728 Kincaid, C., Olson, P., 1987. An experimental study of subduction and slab migration. J.
729 Geophys. Res. 92, 13,832–13,840.
730 Korenaga, J., Karato, S.-I., 2008. A new analysis of experimental data on olivine rheology. J.
731 Geophys. Res. 113, B02403, doi:10.1029/2007JB005100.
732 Lallemand, S., Heuret, A., Faccenna, C., Funiciello, F., 2008. Subduction dynamics as revealed
733 by trench migration. Tectonics 27, TC3014, doi:10.1029/2007TC002212.
734 Le Pichon, X., Sibuet, J.C., 1971. Western extension of the boundary between European and
735 Iberian plates during the Pyrenean orogeny. Earth Planet. Sci. Lett. 12, 83-88.
736 Lewis, S.L. et al., 2009. Increasing carbon storage in intact African tropical forests. Nature 457,
737 1003–1006.
738 Lu, G., Kaus, B., Zhao, L., Zheng, T., 2015. Self-consistent subduction initiation induced by
739 mantle flow. Terra Nova 27, 130–138. doi:10.1111/ter.12140
740 MacLeod, K.G., Huber, B.T., 1996. Reorganization of deep ocean circulation accompanying a
741 Late Cretaceous extinction event. Nature 380, 422−425.
742 Malhi, Y. et al., 2008, Climate change, deforestation, and the fate of the Amazon. Science 319,
743 169–172.
744 Manabe, S., Stouffer, R.J., 1993. Century-scale effects of increased atmospheric CO_2 on the
745 ocean-atmosphere system. Nature 364, 215−218.
746 Marques, F.O. et al., 2013. Testing the influence of far-field topographic forcing on subduction
747 initiation at a passive margin. Tectonophysics 608, 517−524.
748 Marques, F.O., Cabral, F.R., Gerya, T.V., Zhu, G., May, D.A., 2014a. Subduction initiates at
749 straight passive margins. Geology 42, 331−334.
750 Marques, F.O., Nogueira, F.C.C., Bezerra, F.H.R., de Castro, D.L., 2014b. The Araripe Basin in
751 NE Brazil: An intracontinental graben inverted to a high-standing horst. Tectonophysics 630,
752 251-264.

753 Matos, R.M.D., 1992. The Northeast Brazilian rift system. Tectonics 11, 766–791.
754 May, D.A., Moresi, L., 2008. Preconditioned iterative methods for Stokes flow problems arising
755 in computational geodynamics. Phys. Earth Planet. Int. 171, 33–47.
756 McKenzie, D.P., 1977. The initiation of trenches: a finite amplitude instability. In: Talwani, M.,
757 Pitman III, W.C. (Eds.), Island Arcs, Deep Sea Trenches and Back-arc Basins. American
758 Geophysical Union, Maurice Ewing Series 1, 57–61.
759 Miles, B.W.J., Stokes, C.R., Vieli, A., Cox, N.J., 2013. Rapid, climate-driven changes in outlet
760 glaciers on the Pacific coast of East Antarctica. Nature 500, 563–566.
761 Moss, R.H. et al., 2010. The next generation of scenarios for climate change research and
762 assessment. Nature 463, 747–756.
763 Müller, R.D., Hanna, E., et al., 2013. Ice-sheet mass balance and climate change. Nature 498,
764 51–59.
765 Nikolaeva, K., Gerya, T.V., Marques, F.O., 2010. Subduction initiation at passive margins:
766 numerical modeling. Journal of Geophysical Research 115, B03406,
767 doi:10.1029/2009JB006549.
768 Nikolaeva, K., Gerya, T.V., Marques, F.O., 2011. Numerical analysis of subduction initiation
769 risk along the Atlantic American passive margins. Geology 39, 463-466.
770 Niu, Y., 2014. Geological understanding of plate tectonics: Basic concepts, illustrations,
771 examples and new perspectives. Global Tectonics and Metallogeny, DOI:
772 10.1127/gtm/2014/0009.
773 Niu, Y.L., O'Hara, M.J., Pearce, J.A., 2003. Initiation of subduction zones as a consequence of
774 lateral compositional buoyancy contrast within the lithosphere: A petrologic perspective. J.
775 Petrol. 44, 851–866.

776 Nogueira, F.C.C., Marques, F.O., Bezerra, F.H.R., de Castro, D.L., Fuck, R.A., 2015. Cretaceous
777 intracontinental rifting and post-rift inversion in NE Brazil: insights from the Rio do Peixe
778 Basin. Tectonophysics in press.
779 Passarelli, C.R., Basei, M.A.S., Wemmer, K., Siga Jr., O., Oyhantçabal, P., 2010. Major shear
780 zones of southern Brazil and Uruguay: escape tectonics in the eastern border of Rio de La
781 plata and Paranapanema cratons during the Western Gondwana amalgamation. International
782 Journal of Earth Sciences, Doi:10.1007/s00531-010-0594-2.
783 Rahmstorf, S., 2002. Ocean circulation and climate during the past 120,000 years. Nature 419,
784 207−214.
785 Rahmstorf, S., 1997. Risk of sea-change in the Atlantic. Nature 388, 825−826.
786 Ranalli, G., 1995. Rheology of the Earth, 2nd ed. Chapman & Hall, London.
787 Richoz S. et al., 2012. Hydrogen sulphide poisoning of shallow seas following the end-Triassic
788 extinction. Nature Geosci. 5, 662–667.
789 Rodríguez-González, J., Negredo, A.M., Billen, M.I., 2012. The role of the overriding plate
790 thermal state on slab dip variability and on the occurrence of flat subduction. Geochem.
791 Geophys. Geosys. 13, Q01002.
792 Rodríguez-González, J., Billen, M.I., Negredo, A.M., 2014. Non-steady-state subduction and
793 trench-parallel flow induced by overriding plate structure. Earth Planet. Sci. Lett. 401, 227-
794 235.
795 Russo, R.M., Silver, P.G., 1996. Cordillera formation, mantle dynamics, and the Wilson cycle.
796 Geology 24, 511-514.
797 Rosenbaum, G., Lister, G.S., 2004. Neogene and Quaternary rollback evolution of the
798 Tyrrhenian Sea, the Apennines, and the Sicilian Maghrebides. Tectonics 23, TC1013.
799 doi:10.1029/2003TC001518.
800 Schellart, W.P., 2005. Influence of the subducting plate velocity on the geometry of the slab and

migration of the subduction hinge. Earth Planet. Sci. Lett. 231, 197–219.

Schellart, W.P., 2008. Subduction zone trench migration: Slab driven or overriding-plate-driven? Phys. Earth Planet. Inter. 170, 73–88.

Schellart, W.P., 2010. Evolution of subduction zone curvature and its dependence on the trench velocity and the slab to upper mantle viscosity ratio. J. Geophys. Res. 115, B11406, doi:10.1029/2009JB006643.

Schellart, W.P., 2011. A subduction zone reference frame based on slab geometry and subduction partitioning of plate motion and trench migration. Geophys. Res. Lett. 38, L16317, doi:10.1029/2011GL048197.

Schellart, W.P., Freeman, J., Stegman, D.R., Moresi, L., May, D., 2007. Evolution and diversity of subduction zones controlled by slab width. Nature 446, 308–311.

Schellart, W.P., Lister, G.S., Toy, V.G., 2006. A Late Cretaceous and Cenozoic reconstruction of the southwest Pacific region: Tectonics controlled by subduction and slab rollback processes. Earth Sci. Rev. 76, 191–233.

Schellart, W.P., Rawlinson, N., 2010. Convergent plate margin dynamics: New perspectives from structural geology, geophysics and geodynamic modelling. Tectonophysics 483, 4–19.

Schellart, W.P., Stegman, D.R., Farrington, R.J., Moresi, L., 2011. Influence of lateral slab edge distance on plate velocity, trench velocity, and subduction partitioning. J. Geophys. Res. 116, B10408, doi:10.1029/2011JB008535.

Schellart, W.P, Stegman, D., Freeman, J., 2008. Global trench migration velocities and slab migration induced upper mantle volume fluxes: Constraints to find an Earth reference frame based on minimizing viscous dissipation. Earth-Sci. Rev. 88, 118–144.

Schmeling, H. et al., 2008. A benchmark comparison of spontaneous subduction models: Towards a free surface. Phys. Earth Planet. Int. 171, 198–223.

Song, H., Wignall, P.B., Tong, J., Yin, H., 2013. Two pulses of extinction during the Permian-

826 Triassic crisis. Nature Geosci. 6, 52–56.
827 Spakman, W., Hall, R., 2010. Surface deformation and slab–mantle interaction during Banda arc
828 subduction rollback. Nature Geosci. 3, 562−566.
829 Stegman, D., Farrington, R., Capitanio, F., Schellart, W.P., 2010a. A regime diagram for
830 subduction styles from 3-D numerical models of free subduction. Tectonophysics 483, 29–45.
831 Stegman, D.R., Freeman, J., Schellart, W.P., Moresi, L., May, D., 2006. Influence of trench
832 width on subduction hinge retreat rates in 3-D models of slab rollback. Geochem. Geophys.
833 Geosyst. 7, Q03012, doi:10.1029/2005GC001056.
834 Stegman, D.R., Schellart, W.P., Freeman, J., 2010b. Competing influences of plate width and
835 far-field boundary conditions on trench migration and morphology of subducted slabs in the
836 upper mantle. Tectonophysics 483, 46–57.
837 Stern, R.J., 2004. Subduction initiation: Spontaneous and induced. Earth Planet. Sci. Lett. 226,
838 275–292.
839 Stocker, T., Schmittner, A., 1997. Influence of CO_2 emission rates on the stability of the
840 thermohaline circulation. Nature 388, 862−865.
841 Thielmann, M., Kaus, B., 2012. Shear heating induced lithospheric-scale localization: Does it
842 result in subduction? Earth Planet. Sci. Lett. 359-360, 1–13.
843 Tommasi, A., Vauchez, A., Fernandes, L.A.D., Porcher, C.C., 1994. Orogen-parallel strike-slip
844 faulting and synkinematic magmatism in the Dom Feliciano Belt, Southern Brazil. Tectonics
845 13, 421-437.
846 Turcotte, D.L., Schubert, G., 2014. Geodynamics. Cambridge University Press, 3rd Edition.
847 Printed in the USA by Sheridan Books Inc.
848 Vauchez, A., Neves, S.P., Caby, R., Corsini, M., Egydio-Silva, M., Arthaud , M., Amaro , V.E.,
849 1995. The Borborema shear zone system. J. South Am. Earth Sci. 8, 247-266.
850 Vauchez, A., Tommasi, A., 2003. Wrench faults down to the asthenosphere: Geological and

851 geophysical evidence and thermo-mechanical effects. In: Storti, F. Holdsworth, R.E. &
852 Salvini, F. (eds) Intraplate Strike-Slip Deformation Belts, Geol. Soc. London Spec. Publ. 210,
853 15-34.
854 Weertman, J., 1968. Dislocation climb theory of steady state creep. Trans. Amer. Soc. Metals 61,
855 681-694.
856 Wignall, P.B., 2001. Large igneous provinces and mass extinctions. Earth-Science Reviews 53,
857 1-33.
858 Wignall, P.B., Twitchett, R.J., 1996. Oceanic anoxia and the end Permian mass extinction.
859 Science 272, 1155-1158.
860 Yamato, P., Kaus, B., Mouthereau, F., Castelltort, S., 2011. Dynamic constraints on the crustal-
861 scale rheology of the Zagros fold belt, Iran. Geology 39, 815–818.